Global and Stochastic Analysis
Vol. 10 No. 2 (July-December, 2023)

Received: 19th April 2023 *Revised: 16th June 2023* *Accepted: 05th July 2023*

ANALYSIS OF CASSON FLUID FLOW BETWEEN TWO POROUS DISKS WITH STRETCHING MOTION AND MASS TRANSPIRATION

SAMPATH KUMAR V S, DEVAKI B, AND NITYANAND P PAI*

Abstract. In the present study, a semi-analytical solution is obtained for the Casson fluid flow between two porous stretchable disks with mass transpiration. The governing equations are reduced to a non-linear ordinary differential equation using suitable similarity transformations. The solution is obtained using a semi-analytical technique (Homotopy Perturbation Method). The effects of Reynolds number (R), Casson parameter (γ), and mass transpiration (λ) for the flow problems are investigated in detail. The radial and vertical velocity profiles were found for moderately large Reynolds numbers. It is observed that the increase in the values of the Casson parameter suppresses the velocity field. As the Reynolds number increases, a boundary layer behaviour is observed near the wall with constant velocity core flow in the centreline region between two disks for mass suction or lower mass injection. The effects of mass transpiration on the flow are quite different and interesting. The present scheme developed admits a remarkable accuracy and has an analytical structure solution, which helps to compute various physical quantities. The results are obtained through an efficient algorithm for HPM using MATHEMATICA. The results are shown in the form of graphs and tables.

1. Introduction

The flow through stretching boundaries is important in industrial applications. Stretching boundary is widely used in the extrusion process of polymers, plastic, thin films, etc. Based on boundary layer assumptions Sakiadis [9] first proposed the solution for the surface stretching problem. An analytical solution for the two-dimension Navier-Stokes equation was given by Crane [3]. Gupta et al. [4] further explored the Crane problem and found a solution for injection and suction at the wall. They found the exact solution for suction/injection of the surface, including heat transfer aspects, and influenced suction/injection parameters on the flow profile. Wang [16] extended the stretching boundary value problem to a three-dimension.

The significance of poroisty in fluid mechanics is immense as it plays a vital role in characterizing the fluid flow in porous system. Zaturka and Banks [17]

2000 *Mathematics Subject Classification.* 34B15; 76D05.
Key words and phrases. Mathematical Modelling, Partial Differential Equations, Non-linear Boundary Value Problem, Casson Fluid Flow, Semi-Analytical Method,Homotopy Perturbation Method.

studied the combined effect of stretching walls and porosity. Mass transpiration phenomena plays an important role in various industrial application including material separation, micro and ultra filteration, etc. The efficiency and effectiveness of many processes, where a material having different transport coefficient can be analysed using this concept. Tiegang Fang [13] investigated the flow between two coaxial infinite stretching disks. Fang and Zhang [14] extended their work by considering both mass transpiration and stretching motion. The flow over a disk or between disks is popular among researchers because of their applications in engineering, such as rotating disk reactors, heat exchangers, bio-fluids, chemical, and automobile industries. Recently, Awati et al. [1] studied the series solution for the viscous flow between two porous disks and stretching motion in the presence of suction/injection with mass transpiration.

Mathematical models narrating the realistic flow problems often involve non-Newtonian fluids. One of these fluids is Casson fluid. It acts as an elastic solid above threshold shear stress and small shear strain. Casson fluid model is a preferred rheological model for many fluids, including blood and chocolate. [[15], [11]]. Squeezing flow of Casson fluid between two parallel plates is widely studied by various authors [[15], [10]]. Casson fluid over a stretching surface studied by Mukhyopadhyay [12]. The magnetohydrodynamic laminar flow between porous disks studied by Chandrasekhara et al. [2].

The homotopy perturbation method is a powerful mathematical tool to solve various non-linear problems. The technique is straightforward; it requires no small parameter. The solutions obtained are highly accurate even with few iterations [[5], [6], [7], [8]]. Casson fluid flow between two porous disks with stretching motion is yet to be considered. In this paper, we fill out the gap of the flow profile for Casson fluid flow between two stretchable disks considering mass transpiration. Solutions are obtained using Homotopy Perturbation Method.

2. Mathematical Modeling

Consider an axis-symmetric Casson fluid flow between two stretchable infinite disks with a distance $2d$ between them. Let the disks be lie in the plane $z = -d$ and $z = d$. The same velocity proportionate to the radii is applied to both discs to stretch them in the radial direction. This formulation is for infinite stretchable disks; however, it can also be applied to finite stretchable disks of sufficiently large diameters in the region near the central axis by ignoring the edge effects. The disks are assumed to be porous, allowing mass transpiration.

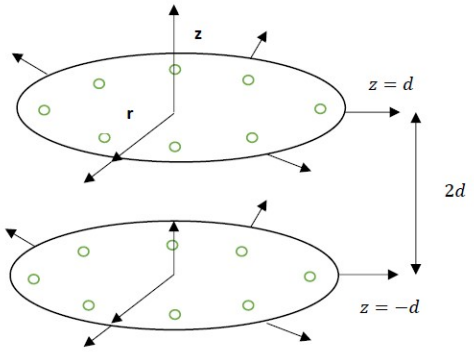

FIGURE 1. Schematic diagram of the problem

The steady state, axis-symmetric Navier Stokes flow equations in the cylindrical coordinates are

$$\frac{1}{r}\frac{\partial}{\partial r}(ru_r) + \frac{\partial u_z}{\partial z} = 0 \tag{2.1}$$

$$u_r\frac{\partial u_r}{\partial r} + u_z\frac{\partial u_r}{\partial z} = -\frac{1}{\rho}\frac{\partial p}{\partial r} + \nu\big(1+\frac{1}{\gamma}\big)\big(\frac{\partial^2 u_r}{\partial r^2} + \frac{1}{r}\frac{\partial u_r}{\partial r} + \frac{\partial^2 u_r}{\partial z^2} - \frac{u_r}{r^2}\big) \tag{2.2}$$

$$u_r\frac{\partial u_z}{\partial r} + u_z\frac{\partial u_z}{\partial z} = -\frac{1}{\rho}\frac{\partial p}{\partial z} + \nu\big(1+\frac{1}{\gamma}\big)\big(\frac{\partial^2 u_z}{\partial r^2} + \frac{1}{r}\frac{\partial u_z}{\partial r} + \frac{\partial^2 u_z}{\partial z^2}\big) \tag{2.3}$$

where $V = (u_r, u_z)$ is the velocity vector. ν, γ, p and ρ are the kinematic viscosity, Casson parameter, fluid pressure, and the density of the fluid respectively. The similarity transformations are

$$u_r = rEF(\eta) \tag{2.4}$$

$$u_z = EdH(\eta) \tag{2.5}$$

$$p = \rho E\nu\big[P(\eta) + \frac{\beta r^2}{4d^2}\big] + P_0 \tag{2.6}$$

here the pressure at the bottom disk is called as the reference pressure denoted by P_0 and $\eta = \frac{z}{d}$, the similarity variable. In this work, the definition of η is not a real similarity variable, but a non- dimensional distance. This definition is formed on the flow characteristics of the considered configuration. The quantity E is the disk stretching strength parameter with a unit $\frac{1}{s}$, and β is a parameter corresponding to pressure gradient for the radial pressure. Substitute equation (2.4) into equations (2.1, 2.2) and (2.3) gives a similarity group of equations as follows

$$H' = -2F \tag{2.7}$$

$$\big(1+\frac{1}{\gamma}\big)F'' - \beta = R(F^2 + F'H) \tag{2.8}$$

$$P' = 2RFH - 2\big(1+\frac{1}{\gamma}\big)F' \tag{2.9}$$

with boundary conditions

$$H(-1) = -\lambda, H(1) = \lambda, F(1) = 1, F(-1) = 1, P(-1) = 0. \tag{2.10}$$

If h and $U_c = Ed$ are the characteristic length and velocity, the Reynolds number is denoted by $R = \frac{Ed^2}{\nu}$. Here ν is the fluid kinematic viscosity. The parameter λ illustrates the mass transpiration strength at the two disks (symmetry assumed). The Reynolds number indicates the disk stretching strength for given d and ν and also the mass transpiration velocity strength for a given λ. $\lambda > 0$ indicates mass suction at the disks and $\lambda < 0$, a mass injection. Substitute equation (2.7) into equation (2.8) gives

$$\big(1 + \frac{1}{\gamma}\big)H''' + \beta - RHH'' + \frac{RH'^2}{2} = 0 \tag{2.11}$$

with the associated boundary conditions as

$$H'(1) = -2, H'(-1) = -2, H(1) = \lambda H(-1) = -\lambda. \tag{2.12}$$

Taking derivative of equation (2.11) with respect to η, we obtain

$$\big(1 + \frac{1}{\gamma}\big)H'''' - RHH''' = 0 \tag{2.13}$$

with the same boundary conditions as in equation (2.12).

3. Method of Solution

The problem is solved using a semi-analytical technique named Homotopy Perturbation Method (HPM). To illustrate the solution of HPM solution for a nonlinear differential equation, let us take,

$$E[f(\xi)] - f_1(\xi) = 0 \tag{3.1}$$

where $E, \xi, f(\xi)$ and f_1 represent the operator, independent variable, unknown function, and a known function. E can be also expressed as

$$E = L + N$$

where L, N are the simple linear part and the remaining part of the equation (3.1).

With the right choice of L, N, homotopy equation can be obtained. The homotopy equation is of the form

$$H(\phi(n, q; q)) = (1 - q)[L(\phi, q) - L(v_0(\xi))] + q[E(\phi, q) - f_1(\xi)] = 0 \tag{3.2}$$

Here q is called an embedding parameter and its value of q varies from zero to unity. The initial guess to the equation (3.1) is $v_0(\xi)$. So we assume the solution of equation (3.2) as follows

$$\phi(n, q) = \sum_{n=0}^{\infty} q^n f_n(\xi) \tag{3.3}$$

The solution to the considered problem is equation (3.3) at $q = 1$ [5].

The zeroth, first and second order solutions of the considered problem are as follows

$$H_0(\eta) = \frac{1}{2}\big[2\eta - 2\eta^3 + 3\eta\lambda - \eta^3\lambda\big] \tag{3.4}$$

$$H_1(\eta) = \frac{1}{560}\Big(\frac{\gamma}{1+\gamma}\Big)\big[-20\eta + 44\eta^3 - 28\eta^5 + 4\eta^7 - 48\eta\lambda + 100\eta^3\lambda \\ -56\eta^5\lambda + 4\eta^7\lambda - 19\eta\lambda^2 + 39\eta^3\lambda^2 - 21\eta^5\lambda^2 + \eta^7\lambda^2\big] \tag{3.5}$$

$$H_2(\eta) = \frac{1}{7761600}\frac{\gamma^2}{(1+\gamma)^2}\big[-2400\eta + 21128\eta^3 - 44352\eta^5 + 36432\eta^7 - 1232\eta^9 \\ +1512\eta^{11} + 3792\eta\lambda + 5879\eta^3\lambda - 155232\eta^5\lambda + 121176\eta^7\lambda - 308300\eta^9\lambda \\ +2268\eta^{11}\lambda + 22224\eta\lambda^2 + 37406\eta^3\lambda^2 - 160776\eta^5\lambda^2 + 121572\eta^7\lambda^2 - 21560\eta^9\lambda^2 \\ +1134\eta^{11}\lambda^2 + 9864\eta\lambda^3 + 6645\eta^3\lambda^3 - 47124\eta^5\lambda^3 \\ +35046\eta^7\lambda^3 - 4620\eta^9\lambda^3 + 189\eta^{11}\lambda^3\big] \tag{3.6}$$

$$H_3(\eta) = \frac{1}{565044800(1+\gamma)^3}R^3\gamma^3\big[3024240\eta - 1790960\eta^3 - 16492112\eta^5 \\ +34959184\eta^7 - 31311280\eta^9 + 14875952\eta^{11} - 3618160\eta^{13} \\ +353136\eta^{15} + 18982128\eta\lambda - 21796480\eta^3\lambda - 69039152\eta^5\lambda \\ +165565920\eta^7\lambda - 141181040\eta 9\lambda + 57616832\eta^{11}\lambda - 10854480\eta^{13}\lambda \\ 706272\eta^{15}\lambda + 36914160\eta\lambda^2 - 59222920\eta^3\lambda^2 - 94740464\eta^5\lambda^2 \\ +275765880\eta^7\lambda^2 - 224784560\eta^9\lambda^2 + 76392680\eta^{11}\lambda^2 - 10854480\eta^{13}\lambda^2 \\ +529704\eta^{15}\lambda^2 + 24526020\eta\lambda^3 - 52291552\eta^3\lambda^3 - 49189140\eta^5\lambda^3 \\ +189251192\eta^7\lambda^3 - 148568420\eta^9\lambda^3 + 40618032\eta^{11}\lambda^3 - 4522700\eta^{13}\lambda^3 \\ +176568\eta^{15}\lambda^3 + 5218221\eta\lambda^4 - 13952671\eta^3\lambda^4 - 8508591\eta^5\lambda^4 \\ +44194917\eta^7\lambda^4 - 33778745\eta^9\lambda^4 + 7483203\eta^{11}\lambda^4 \\ -678405\eta^{13}\lambda^4 + 22071\eta^{15}\lambda^4\big] \tag{3.7}$$

4. Results and Discussion

The effects of Reynolds number, mass transpiration parameter and Casson parameter on the fluid flow profile are discussed in this section. The velocity profiles are obtained using HPM, which are drawn only between $\eta = 0$ and $\eta = 1$ because of the symmetry at $\eta = 0$ for different values of γ, λ, and R. The impact of different values of R with $\gamma = 0.3$ on velocity profile for no mass transpiration ($\lambda = 0$) is demonstrated in Figure 2. The vertical velocity curve is linear near the central region and decreases with an increase in R. We note that the radial velocity increases in the region $0 \leq \eta \leq 0.5$ and decreases in $0.5 \leq \eta \leq 1$.

Figure 3 shows the velocity profiles for various values of R, $\gamma = 0.2$ for mass suction ($\lambda = 2$). The vertical velocity is observed to be decreased as there is an increase in R. The radial velocity profile nature was found to be the same as the no mass transpiration case. Figure 4 depicts the effect of different values of R

and $\gamma = 0.2$ on the velocity profile with mass injection ($\lambda = -5$). The vertical velocity is observed to be decreasing as we increase R. It is also noted that radial velocity increased in the region $0 \leq \eta \leq 0.4$, and an opposite trend is noted in the $0.4 \leq \eta \leq 1$ region.

Figures 5 and 6 represent the mass suction effect on the velocity profile with $\gamma = 0.2$ for $R = 0.1$ and $R = 2$, respectively. The magnitude of vertical velocity increase with an increase of λ, and a reverse behavior is noted in the case of the radial velocity profile. Figures 7 and 8 show the effect of mass injection for $R = 0.1$ and $R = 2$, respectively, for $\gamma = 0.2$. The nature of the corresponding curves was found to be opposite to that of the mass suction case.

The impact of the Casson parameter on the velocity profile for $R = 10$ is shown in Figure 9. It demonstrates the suppression of vertical velocity as there is an increase in γ. The radial velocity is found to be increasing in $0 \leq \eta \leq 0.5$ and decreasing in $0.5 \leq \eta \leq 1$ region. Table 1 shows the wall shear stress $H''(1)$ for different values of λ, γ and R. The values of $H''(1)$ is found to be decreasing with an increase of the mass transpiration parameter and the Reynolds number. We can also observe the suppression of wall shear stress for increment in the Casson parameter.

TABLE 1. Wall shear stress $H''(1)$

γ	λ	$R = 0$	$R = 1$	$R = 2$	$R = 5$	$R = 10$
0.1	-5	9	8.69790	8.42858	7.78808	7.12565
	-3	3	2.94217	2.88802	2.74571	2.56463
	-1	-3	-2.98713	-2.97449	-2.93789	-2.88108
	1	-9	-9.10275	-9.20843	-9.54320	-10.16080
	3	-15	-15.41800	-15.86760	-17.41560	-20.69080
	5	-21	-21.94680	-23.01000	-26.45290	-36.12470
0.2	-5	9	8.47132	8.04451	7.20996	6.54524
	-3	3	2.89680	2.80542	2.59064	2.37235
	-1	-3	-2.97658	-2.95391	-2.89021	-2.79688
	1	-9	-9.19062	-9.39112	-10.05260	-11.35430
	3	-15	-15.79050	-16.69000	-20.08390	-28.01080
	5	-21	-22.82440	-25.05690	-34.37830	-55.53660
0.3	-5	9	8.29608	7.77451	6.90347	4.06303
	-3	3	2.86032	2.74243	2.49014	2.27396
	-1	-3	-2.96777	-2.93698	-2.85252	-2.73458
	1	-9	-9.26656	-9.55213	-10.52410	-12.51710
	3	-15	-16.12320	-17.49530	-22.81470	-35.45830
	5	-21	-23.6329	-27.06940	-42.27290	-69.75080

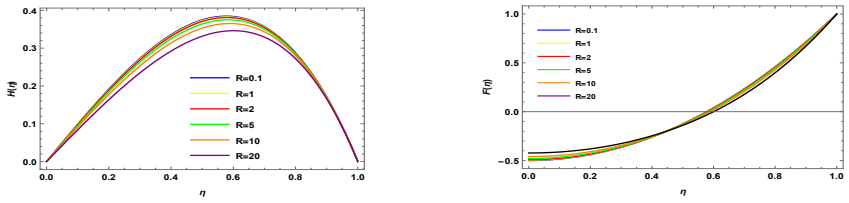

(A) (B)

FIGURE 2. (A) Vertical and (B) Radial velocity profiles for for different R when $\gamma = 0.3$ and $\lambda = 0$.

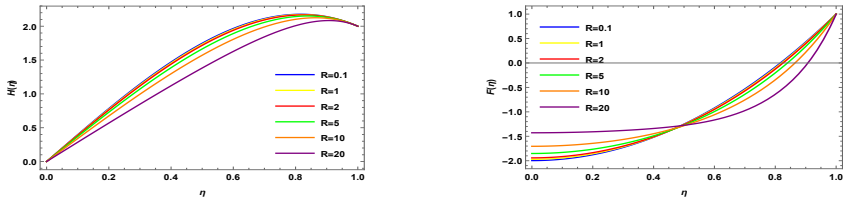

(A) (B)

FIGURE 3. (A) Vertical and (B) Radial velocity profiles for different R when $\gamma = 0.2$ and $\lambda = 2$

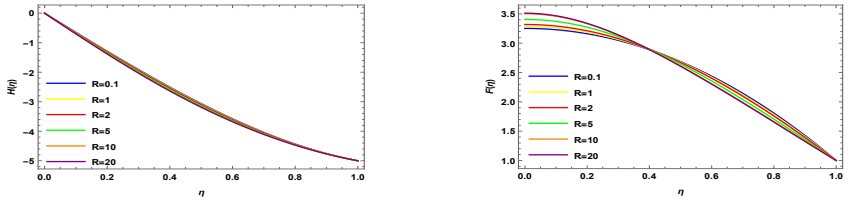

(A) (B)

FIGURE 4. (A) Vertical and (B) Radial velocity profiles for different R when $\gamma = 0.2$ and $\lambda = -5$

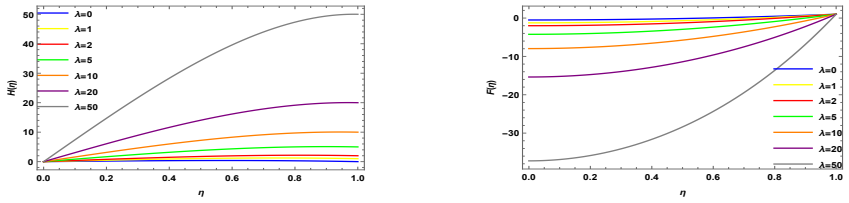

(A) (B)

FIGURE 5. (A) Vertical and (B) Radial velocity profiles for different positive mass transpiration strength when $\gamma = 0.2$ and $R = 0.1$.

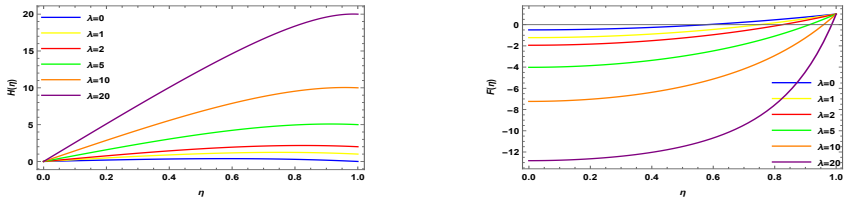

(A) (B)

FIGURE 6. (A) Vertical and (B) Radial velocity profiles for different positive mass transpiration strength when $\gamma = 0.2$ and $R = 2$.

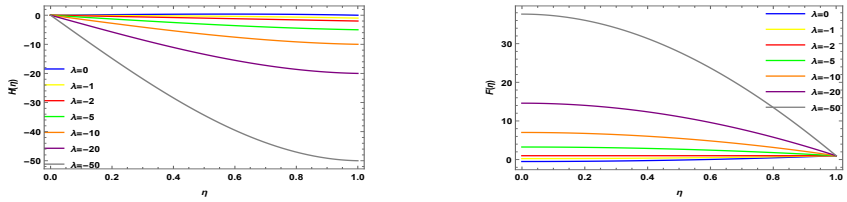

(A) (B)

FIGURE 7. (A) Vertical and (B) Radial velocity profiles for different negative mass transpiration strength when $\gamma = 0.2$ and $R = 0.1$.

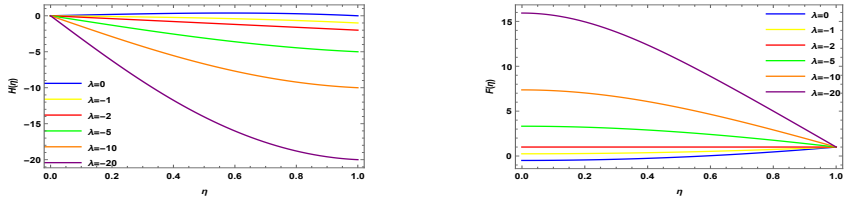

(A) (B)

FIGURE 8. (A) Vertical and (B) Radial velocity profiles for different negative mass transpiration strength when $\gamma = 0.2$ and $R = 2$.

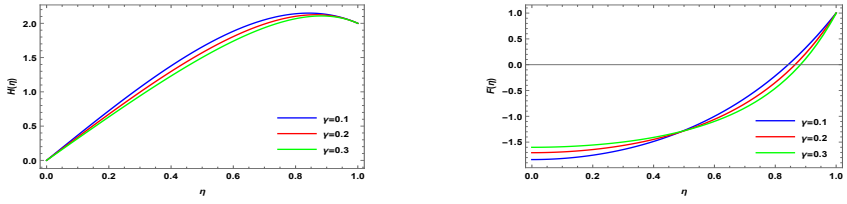

(A) (B)

FIGURE 9. (A) Vertical and (B) Radial velocity profiles for different Casson parameter when $\lambda = 2$ and $R = 10$.

5. Conclusion

In this paper we have analysed the semi-analytical solution for the Casson fluid flow between two porous stretchable disks with mass transpiration. We have obtained the effects of mass transpiration parameter, Reynolds number and Casson parameter on the fluid flow with the help of homotopy perturbation method. HPM is flexible and very efficient method to solve non-linear differential equation. This approach reveals the analytical structure of the solution. Contrary to numerical schemes, where each scheme must be developed separately, the resultant quantity can be produced quickly and efficiently. The proposed method requires less storage space and time.

References

1. Awati, V. B., Jyoti, Manjunath and Bujurke, N. M.: Series solution of steady viscous flow between two porous disks with stretching motion, *Journal of Nanofluids* **7(5)** (2018) 982–994.
2. Chandrasekhara, B. and Rudraiah, N.: Magnetohydrodynamic laminar flow between porous disks, *Applied Scientific Research* **23(1)** (1971) 42–52.
3. Crane, L. J.: Flow past a stretching plate, *Zeitschrift für angewandte Mathematik und Physik ZAMP* **21(4)** (1970) 645–647.
4. Gupta, P. S. and Gupta, A. S.: Heat and mass transfer on a stretching sheet with suction or blowing, *The Canadian Journal of Chemical Engineering* **55(6)** (1977) 744–746.
5. Ji-Huan, He: Homotopy perturbation technique, *Computer methods in applied mechanics and engineering* **178(3)** (1999) 257–262.
6. Ji-Huan, He: Homotopy perturbation method: a new nonlinear analytical technique, *Applied Mathematics and computation* **135(1)** (2003) 73–79.
7. Ji-Huan, He: Recent development of the homotopy perturbation method, *Topological methods in nonlinear analysis* **31(2)** (2008) 205–209.
8. Ji-Huan, He: An elementary introduction to the homotopy perturbation method, *Computers and Mathematics with Applications* **57(3)** (2009) 410–412.
9. Sakiadis, B. C.: Boundary-layer behavior on continuous solid surfaces:I boundary-layer equations for two-dimensional and axisymmetric flow, *AIChE Journal* **7(1)** (1961) 26–28.
10. Sampath Kumar, V. S., N. P., Pai and Devaki, B.: Analysis of MHD flow and heat transfer of laminar flow between porous disks, *Frontiers in Heat and Mass Transfer* **16(3)** (2021) 1–7.
11. Swati Mukhopadhyay, Prativa Ranjan De, Krishnendu Bhattacharyya, and Layek G.C.: Casson fluid flow over an unsteady stretching surface, *Ain Shams Engineering Journal* **4(4)** (2013) 933–938.
12. Swati Mukhopadhyay: Casson fluid flow and heat transfer over a nonlinearly stretching surface, *Chinese Physics B* **22(7)** (2013) 74701–74708.
13. Tiegang, Fang and Ji, Zhang: Flow between two stretchable disks-an exact solution of the navier-stokes equations, *International Communications in Heat and Mass Transfer* **35(1)** (2008) 892–895.
14. Tiegang, Fang and Xin, He: Steady Viscous Flow Between Two Porous Disks With Stretching Motion, *Journal of Fluids Engineering* **138(1)** (2015) 11201–11207.
15. Umar Khan, Naveed Ahmed, SIU Khan, Saima Bano, and Syed Tauseef, Mohyud-Din: Unsteady squeezing flow of a casson fluid between parallel plates, *World Journal of Modelling and Simulation* **10(4)** (2014) 308–319.
16. Wang, C. Y.: The three-dimensional flow due to a stretching flat surface, *The Physics of Fluids* **27(8)** (1984) 1915–1917.
17. Zaturska, M. B. and Banks, W. H. H.: New solutions for flow in a channel with porous walls and/or non-rigid walls, *Fluid Dynamics Research* **33(1)** (2003) 57–65.

SAMPATH KUMAR V S: DEPARTMENT OF MATHEMATICS, MANIPAL INSTITUTE OF TECHNOLOGY, MANIPAL ACADEMY OF HIGHER EDUCATION, MANIPAL, KARNATAKA-576104, INDIA
Email address: sampath.kvs@manipal.edu

DEVAKI B: DEPARTMENT OF MATHEMATICS, MANIPAL INSTITUTE OF TECHNOLOGY, MANIPAL ACADEMY OF HIGHER EDUCATION, MANIPAL, KARNATAKA-576104, INDIA
Email address: devaki.badekkila@learner.manipal.edu

NITYANAND P PAI: DEPARTMENT OF MATHEMATICS, MANIPAL INSTITUTE OF TECHNOLOGY, MANIPAL ACADEMY OF HIGHER EDUCATION, MANIPAL, KARNATAKA-576104, INDIA
Email address: nithyanand.pai@manipal.edu *Corresponding author